

# **Growth of colloidal nanoparticles of group II-VI and IV-VI semiconductors on top of magnetic iron-platinum nanocrystals**

Marco Zanella<sup>1,2</sup>, Andrea Falqui<sup>3</sup>, Stefan Kudera<sup>2,4,5</sup>, Liberato Manna<sup>4</sup>, Maria F. Casula<sup>3,\*</sup>, Wolfgang J. Parak<sup>1,2,\*</sup>

<sup>1</sup> Fachbereich Physik, Philipps Universität Marburg, Marburg, Germany

<sup>2</sup> Center for Nanoscience, Ludwig Maximilians Universität München, München, Germany

<sup>3</sup> Dipartimento di Scienze Chimiche and INSTM, Università di Cagliari, Cagliari, Italy.

<sup>4</sup> National Nanotechnology Laboratory of CNR-INFM, Lecce, Italy.

<sup>5</sup> Max Planck Institute for Metals Research, Dept. New Materials and Biosystems & University of Heidelberg, Dept. of Biophysical Chemistry, postal address: Heisenbergstr. 3, D-70569 Stuttgart, Germany

\* corresponding authors: casulaf@unica.it, wolfgang.parak@physik.uni-marburg.de

## **Supporting Information**

### **I) Synthesis**

I.1) Chemicals

I.2) FePt synthesis

I.3) General concept for growing hybrid particles

I.4) FePt/S and FePt/Se synthesis

I.5) FePt-CdS synthesis

I.6) FePt-ZnS synthesis

I.7) FePt-PbS synthesis

I.8) FePt-CdSe synthesis

I.9) FePt-ZnSe synthesis

I.10) FePt-PbSe synthesis

I.11) Comparison of the reaction conditions

### **II) Characterization of structural properties**

II.1) X-ray diffraction (XRD)

II.2) High Resolution transmission electron microscopy (HREM)

### **III) Characterization of optical properties**

### **IV) Characterization of magnetic properties**

### **V) References**

## **I) Synthesis**

### **I.1) Chemicals**

Octyl ether (99%), hexadecanediol (Tech 90%) and iron pentacarbonyl (99.99%), oleic acid (Tech 90%), oleyl amine (Tech 70%), sulphur (100Mesh sublimed) and selenium (99,99% 100Mesh) powder were purchased from Sigma. Tri-n-octylphosphine oxide (TOPO, 98%) was purchased from Alpha Aesar and cadmium acetylacetonate (98%, “water free”), zinc acetylacetonate (98%), lead acetylacetonate (min 95%), and platinum acetylacetonate (98%) were purchased from Strem. All solvents used for precipitation and re-dispersion of the particles (methanol, ethyl acetate, chloroform, toluene and hexane) were purchased as anhydrous solvents from Sigma. Before any synthesis Zinc acetylacetonate was dried under vacuum for 1h at ca. 100°C and then stored under inert atmosphere. All other reactants were used as delivered. The metal compounds and the chalcogens were handled only under inert (nitrogen) atmosphere.

### **I.2) FePt synthesis**

For the synthesis of the iron platinum cores we followed the recipe previously reported by Sun [1]. In a 50 ml three neck flask 10 ml of octyl ether, 95 mg of platinum acetylacetonate and 195 mg of hexadecanediol were mixed under nitrogen atmosphere. The temperature was raised to 100°C until the solution turned into clear translucent yellow color. A mixture of oleic acid (0.8 ml), oleyl amine (0.8 ml), and iron pentacarbonyl (0.6 ml) was injected quickly under vigorous stirring into the platinum acetylacetonate solution. The temperature was then increased to 280°C at a controlled rate of 12°C/min. The solution was left at that temperature for 15 more minutes. Finally the heating mantle was removed to stop the reaction.

### **I.3) General concept for growing hybrid particles**

The further formation of heterodimers discussed in this work can be divided into three steps as described by Gu et al. [2]. In a first step, an amorphous shell of either sulphur or selenium was formed on FePt nanocrystals. In a second step, a metal (cadmium, zinc or lead) was added to this shell, which at this stage still was amorphous. In the last step a single, crystalline domain was formed out of the amorphous shell. This step can be understood as a dewetting process in which the shell material retracts into a single bleb. The entire reaction from the synthesis of the FePt nanocrystals to the formation of the dimers was carried out in a single pot. No washing steps are involved. In this study we also stopped the synthesis after the individual steps, in order to perform further characterization of the sample at the different stages of growth. In this case the nanoparticles were purified as follows: the reaction solution was cooled to room temperature and methanol and a small quantity of ethyl acetate were added to it in order to precipitate the nanoparticles. The ethyl acetate was necessary to enable mixing of the methanol with the reaction solution. After centrifugation the nanoparticles could be collected as a precipitate. Further purification steps involved the re-dispersion of the nanoparticles in a non-polar solvent such as chloroform, toluene or hexane and the subsequent precipitation with methanol. With these three non-polar solvents no further addition of ethyl acetate was necessary. The samples were characterized either after the first precipitation or after several further redispersion/precipitation cycles.

#### I.4) FePt/S and FePt/Se synthesis

FePt/S nanocrystals were synthesized by following the recipe reported by Gu [2]. Once the iron-platinum nanoparticles were prepared as described above, the reaction solution was cooled down to 100°C and 5 mg of sulphur powder were added under vigorous stirring. Since the whole synthesis was performed in a dry box we could add the powder by simply removing the septum from the flask and pouring the powder into the FePt NCs solution. With the help of a syringe remaining sulphur sticking to the flask was removed by rinsing the walls with nanoparticle solution. After 5min FePt/S nanoparticles were formed (Figure SI-1).

For the characterization of FePt/S the particles then were precipitated from the solution by addition of anhydrous methanol (15ml) and a small quantity of ethyl acetate (2-3 ml) in order to prevent phase separation of the solvents. The supernatant was discarded, and the precipitate could be re-dispersed in chloroform, toluene or hexane. If the precipitation of these particles was performed at a moderate speed (800RPM) the re-dispersed solution was stable for months.

With a similar procedure we could synthesize FePt/Se nanocrystals. In this case 12 mg of Se powder were injected (as described before) into the FePt nanocrystals solution at 150°C. The solution was left stirring at that temperature for 12-14 min.

For characterization the solution was cooled down to room temperature and precipitated following the protocol described above. A small insoluble fraction of the nanocrystals was found after the re-dispersion and was discarded as precipitate after additional centrifugation<sup>1</sup>.

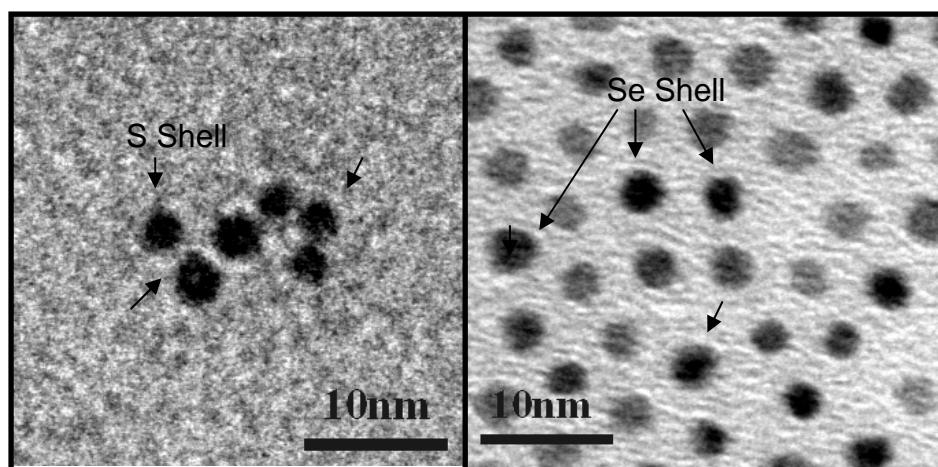


**Figure SI-1:** Low magnification TEM image of FePt/S (left) and FePt/Se (right) nanoparticles. Insets show a higher magnification of the same samples. The dark dots are iron platinum particles, while the light gray shell around them is the chalcogenic shell. The scale bars correspond to 10 nm.

<sup>1</sup> TEM characterization of this insoluble precipitate showed that it was made of big agglomerates of FePt/Se nanocrystals. We can speculate that these agglomerates formed as by-product either directly during the shell formation or by the stripping off of the surfactants from the nanocrystals' surface occurring during the purification.

## I.5) FePt-CdS synthesis

FePt/S nanocrystals were prepared as described in I.4. However, instead of precipitating the FePt/S particles from the solution at the end of the reaction, 1g TOPO, 105mg of hexadecanediol and 50mg of cadmium acetylacetonate were added to the hot reaction solution. These chemicals were added consecutively to the solution following the same approach used for the S and Se addition, thus pouring most of the powder into the flask and rinsing the remaining powder with about 1-2ml of nanoparticles solution. After 10 min FePt/CdS core/shell particles were formed. At that point the CdS shell was still amorphous. In order to anneal the crystalline structure, the temperature was risen from 100°C to 260-270°C at a rate of 5°C per minute. Once 260-270°C were reached, the heating mantel was removed and the solution was allowed to cool to room temperature. Dimers were precipitated by centrifugation as described in section I.4. Before characterization, the precipitate was redispersed in chloroform and washed once by precipitation with methanol and subsequent re-dispersion.

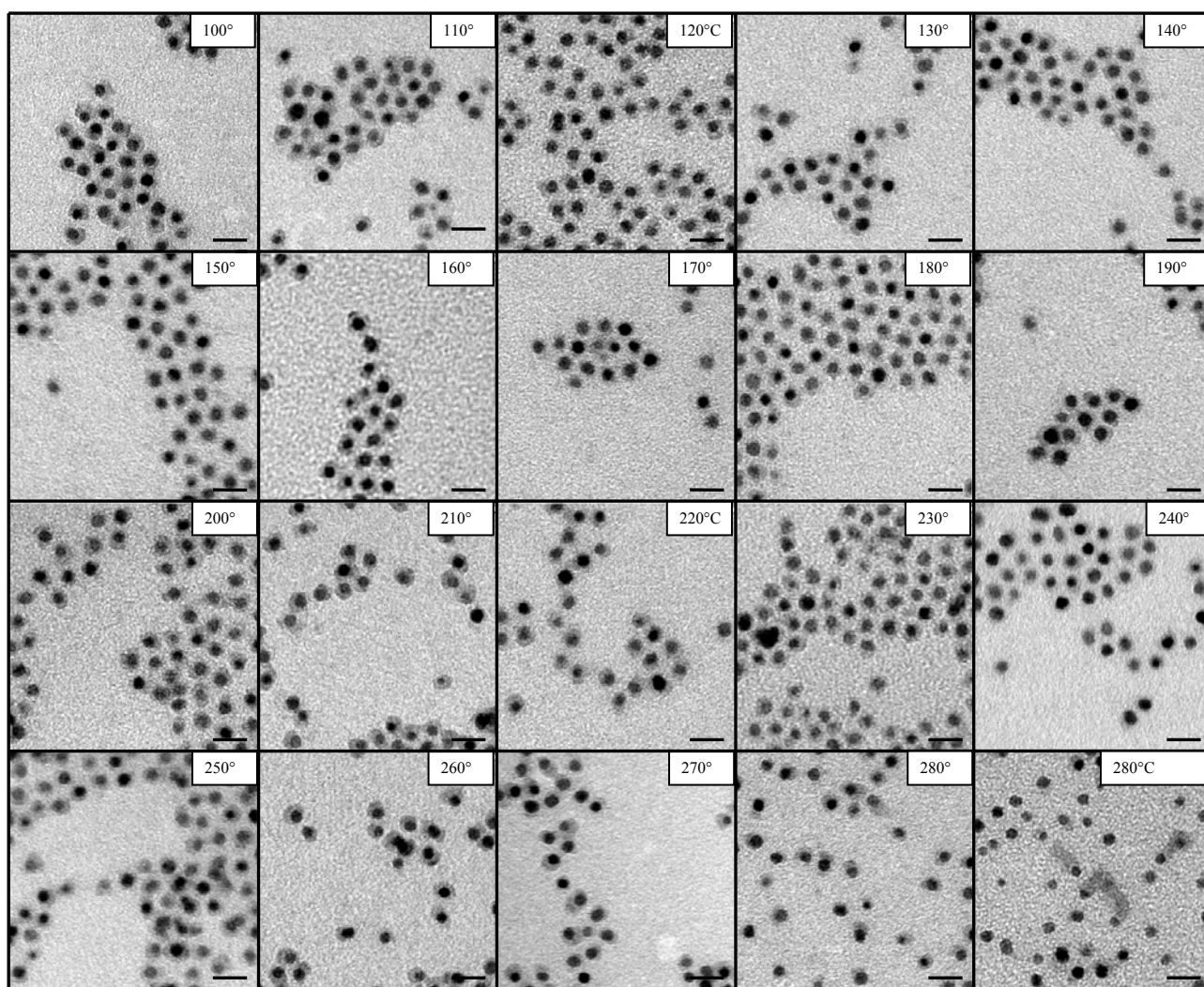


**Figure SI-2:** TEM micrographs of FePt-CdS particles at different stages of the annealing process. After the synthesis of the FePt/CdS core/shell particles at 100°C (time 0min) the solution temperature was raised to 280°C at a rate of 5°C/min. About 1ml of the hot nanoparticles solution was taken from the flask every 2 min with a glass syringe and left to cool down to room temperature. This solution was then purified with methanol and ethyl acetate as described above. The precipitate was re-dispersed in chloroform and TEM samples were prepared by depositing a drop of nanoparticles solution on a TEM grid. The image “280°C+2min” is referred to a sample in which the solution temperature was left at 280°C for 2 more minutes after the annealing ramp. Scale bars correspond to 10 nm.

### I.6) FePt-ZnS synthesis:

The synthesis of FePt/ZnS nanoparticles followed the same route as for the synthesis of the FePt/CdS (see I.5), only that cadmium was replaced by zinc. TOPO (1g), hexadecanediol (105 mg) and dried zinc acetylacetonate (40 mg) were consecutively injected in the hot solution (100°C) of FePt/S nanoparticles and left reacting for 10min. For characterization of the FePt/ZnS core/shell particles the sample was washed once as described above by performing two cycles of precipitation and re-dispersion.

For the growth of FePt-ZnS dimers the core/shell particles solution temperature was raised to 260-270°C at a rate of 5°C/min. Annealing of the FePt/ZnS particles led to the formation of dimers composed of a FePt and a ZnS domain. Keeping the solution at high temperature for a longer time produced unstable solutions as in the case of cadmium-containing dimers (See rightmost image in Figure SI-3).

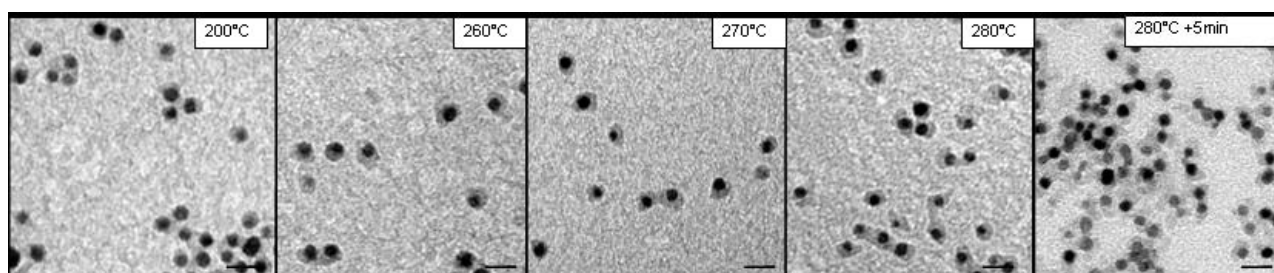


**Figure SI-3:** TEM micrographs of FePt-ZnS particles at different stages of the annealing process. The scale bars correspond to 10nm.

### I.7) FePt-PbS synthesis:

The synthesis of FePt-PbS nanoparticles needed a "softer" approach as compared to the one used for the addition of ZnS and CdS blebs. After the formation of the FePt/S nanoparticles at 100°C the mantle was removed and the solution was allowed to cool to room temperature. When the solution reached 80-90°C TOPO (1 g) and hexadecanediol (105 mg) were added and left dissolving. When the temperature reached 35-40°C lead acetylacetonate (40mg) was added and left reacting for about 5min to form FePt/PbS cores/shell particles.

The formation of the FePt-PbS dimers from the core/shell particles was performed by heating the core/shell particles solution to 130-140°C at a rate of 0.6°C/min without any purification step after the synthesis of the of the core/shell particles. The annealing of the FePt/PbS particles led to the formation of FePt-PbS dimers having one iron platinum domain combined with a PbS one. Keeping the solution at high temperature for a longer time resulted in unstable solutions as in the case of CdS and CdSe.

### I.8) FePt-CdSe synthesis:

FePt/CdSe core/shell nanoparticles were prepared starting from FePt/Se nanoparticles (see section I.4). The further processing was the same as in the case of FePt/CdS core/shell particles, yet the temperature profile of the reaction was different. Cadmium acetylacetonate along with TOPO and hexadecanediol was added at 150°C. After 10min at that temperature the solution was cooled down

to room temperature. For characterization the FePt/CdSe core/shell particles were precipitated with methanol and ethyl acetate, following the same procedure as described above.

For the formation of FePt-CdSe dimers the FePt/CdSe core/shell nanocrystals, without any purification step, were annealed and dewetting started at around 150°C. The heating rate was the same as used for the FePt-CdS dimers. TEM and structural analysis displayed the formation of FePt-CdSe dimers at 260-270°C. In these samples most of the particles in solution are dimers, while few particles are made of two iron platinum particles connected by a cadmium selenide part, together with a little precipitate. This precipitate was removed with by further centrifugation of the redispersion and by collecting the supernatant.

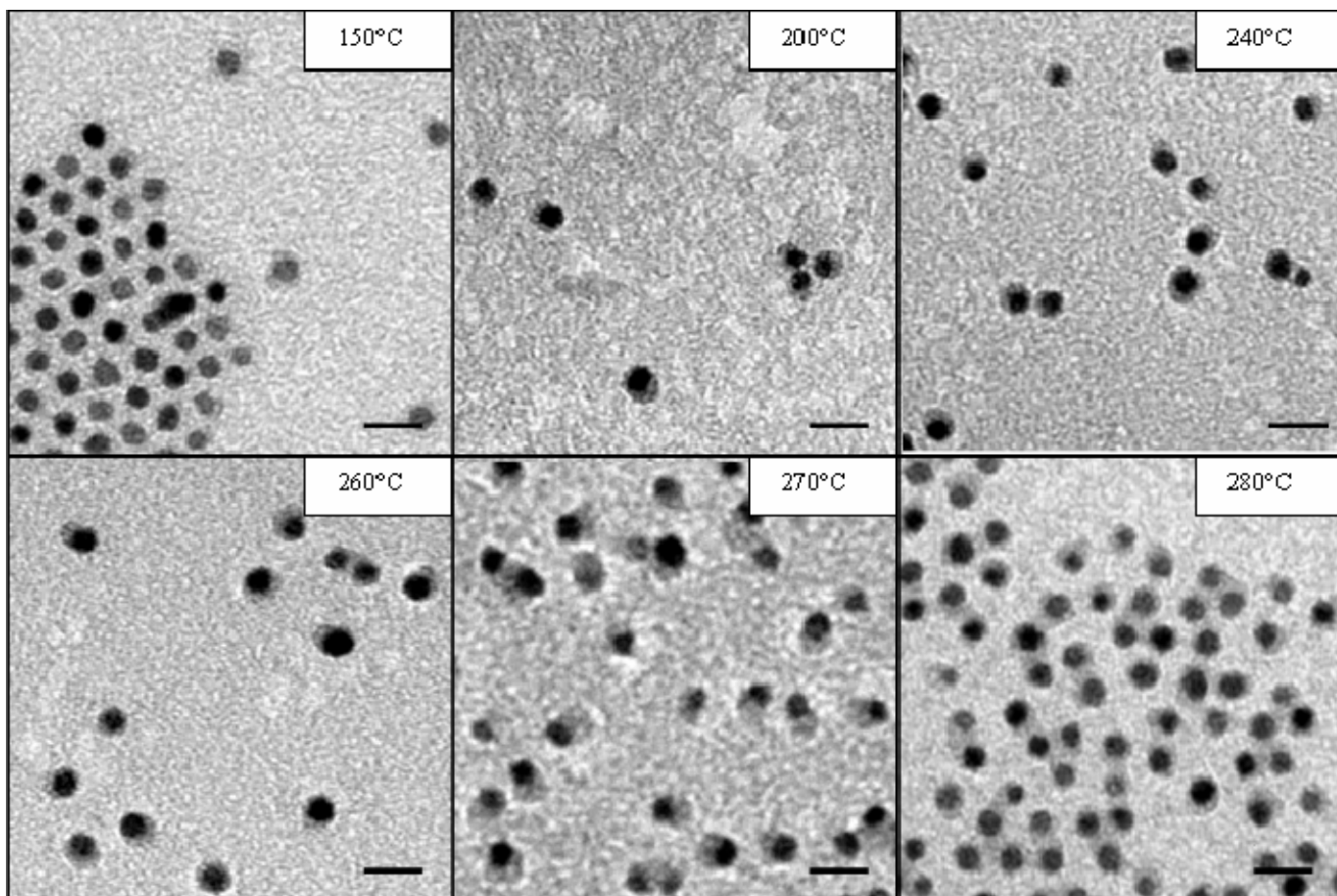


**Figure SI-4:** FePt-ZnS particles at different stages of the annealing process. The scale bars correspond to 10nm.

### I.9) FePt-ZnSe synthesis:

After the synthesis of FePt/Se core/shell nanocrystals at 150°C the solution was left cooling down at room temperature to 35-40°C. During the cooling, at about 100°C, TOPO (1g) and hexadecanediol (105mg) were added to the solution in order to favor their dissolution. Once the temperature had reached 35-40°C Zn(acac)<sub>2</sub> (40mg) was added and let reacting for about 5min.

It turned out that the addition of zinc acetylacetonate to a solution of FePt/Se NCs at 35°C etches away the selenium layer from the magnetic cores, so that no FePt/ZnSe core/shell particles could be formed.

### **I.10) FePt-PbSe synthesis:**

After the synthesis of FePt/Se nanocrystals at 150°C the solution was left to cool down to 35-40°C. During the cooling, at about 100°C TOPO (1g) and hexadecanediol (105mg) were added to the solution in order to favor their dissolution. Once at 35-40°C Pb(acac)<sub>2</sub> (65mg) was added and let reacting for 3-5min.

The addition of lead acetylacetonate to a solution of FePt/Se NCs at 35°C caused etching away of the selenium layer from the magnetic cores and in addition caused the formation of PbSe agglomerates including an unspecified number of FePt particles. In some cases the PbSe agglomerates include just one FePt particle forming a dimer-like structure with a semiconductor part of different size. Several iron platinum particles seem to be without any shell (i.e. the Se has been etched away), but we cannot exclude that a thin layer or little crystals of PbSe might surround or stick to the magnetic core like the tiny drops of liquid left on a finger tip when dewetting occurs too quickly. The high reactivity of lead ions with the selenium layer is the main cause which prevents the formation of defined FePt/PbSe core/shell nanostructures. The XRD pattern of the sample (shown in Figure SI-6) indicates the presence of nanocrystalline PbSe, suggesting therefore that crystallization of lead selenide occurs despite the low reaction temperature (30-40°C). As discussed later, along with the FePt and PbSe phases the XRD pattern also suggests the formation of Pb<sub>4</sub>Pt. The formation of the lead-platinum alloy and of the PbSe may involve the platinum acetylacetonate left in solution after the FePt nanocrystals growth and the selenium left in solution after the Se shell formation.

### **I.11) Comparison of the reaction conditions**

For the synthesis of the FePt/S nanoparticles we followed the protocol reported by Gu.[2]. The sulphur powder was dissolved in the iron platinum nanoparticle solution at 100°C and the sulphur atoms were left reacting with the magnetic core surfaces for 5min in order to form an amorphous shell. The reaction of these materials for the formation of the FePt/XS (X= Cd, Zn, Pb) core/shell particles requires quite different conditions due to the different reactivity the X precursors with the sulphur shell. For cadmium acetylacetonate the reaction at 100°C for 5min was already reported by Gu. The same temperature was kept for zinc acetylacetonate, which was left reacting with the sulphur shell for a longer time (about 10 min) in order to allow for a complete reaction of the zinc precursor. When the same dewetting rate used for FePt/CdS was applied to FePt/ZnS, it led to particles with dimer shape at almost 270°C, after which prolonged dewetting led to the formation of big agglomerates. Structural analysis of FePt-ZnS dimers showed that the semiconductor bleb is not yet crystalline. This fact could be due to the lower reactivity of the zinc with sulphur in the shell. When we replaced cadmium with lead at 100°C the product was always found to be unstable. Due to the high reactivity of lead with sulphur low temperature conditions (35-40°C) were required in order to have stable solutions of FePt/PbS particles. To prevent aggregation even the dewetting rate for the dimer formation needed to be very low, about 0.6°C/min versus 5°C/min used for cadmium and zinc.

For the adhesion of selenium on the magnetic nanoparticles a temperature of 150°C was chosen in order to better control the shell growth. This reaction temperature was able to prevent formation of big agglomerates and to minimize the possible doping of the semiconductor material due to the decomposition of the unreacted iron pentacarbonyl. Selenium was left reacting for 12-14min, during which it formed a thin amorphous shell around the iron platinum nanocrystals (Figure SI-1). After the formation of FePt/CdSe core/shell particles the dewetting rate applied for the synthesis of the FePt-CdS dimers led to FePt-CdSe dimers when the temperature had reached 270°C. Moving from

cadmium to zinc and lead precursors ( $\text{Zn}(\text{acac})_2$  and  $\text{Pb}(\text{acac})_2$ ) we observed that not even the low temperature reaction ( $35^\circ\text{C}$ ) allowed for a controlled shell growth.

|  | FePt-CdS | FePt-ZnS | FePt-PbS | FePt-CdSe |
|--|----------|----------|----------|-----------|
| Addition of the S/Se shell                           |          |          |          |           |
| Temperature at S/Se addition [ $^\circ\text{C}$ ]    | 100      | 100      | 100      | 150       |
| Reaction time (chalcogen shell) [min]                | 5        | 5        | 5        | 12-14     |
| Addition of Cd/Zn/Pb                                 |          |          |          |           |
| Reaction time (semiconductor shell) [min]            | 10       | 10       | 5        | 10        |
| Reaction temperature [ $^\circ\text{C}$ ]            | 100      | 100      | 35-40    | 150       |
| Dewetting rate [ $^\circ\text{C}/\text{min}$ ]       | 5        | 5        | 0,6      | 5         |
| Temperature for dimer formation [ $^\circ\text{C}$ ] | 260-270  | 260-270  | 130-140  | 260-270   |

**Table S1.** Summary of the reaction conditions for the synthesis of FePt-CdS, FePt-CdSe, FePt-ZnS and FePt-PbS dimers.

## **II) Structural Characterization:**

### **II.1) X-ray diffraction (XRD)**

XRD patterns were recorded on a X3000 Seifert diffractometer equipped with a graphite monochromator on the diffracted beam. The scans were collected using Cu-K $\alpha$  radiation at 50 kV and 35 mA within the range of 10-100° (2 $\theta$ ). The nanocrystals were precipitated from colloidal solution by addition of ethanol and deposited on a XRD sample holder prior to scan collection. Phase identification was performed by comparison with the Powder Diffraction Files database PDF-2 File [3].

X-Ray diffraction (XRD) patterns were recorded in order to obtain representative information on the average structural features of the samples at the different steps of the dimer growth. Figure SI-5 shows the pattern of the original plain FePt nanocrystals, of FePt-CdS core/shell particles, and of FePt-CdS dimers. As expected, the composite samples show the reflections of the FePt alloy as main contribution with no significant difference in line broadening. Slight differences in the relative ratio of low intensity reflections of the FePt alloy are observed upon heterostructure formation, and likely due to the effect of annealing or ion diffusion which may affect ordering, and slight symmetry or composition variation. In addition, the dimer sample shows an additional feature centered at about 26° (2 $\theta$ ) due to the formation of nanocrystalline CdS which is not present in the core/shell sample. These data, which were also confirmed by selected area electron diffraction (SAED) collected by conventional TEM, indicate that in case of the core/shell particles the CdS shell is amorphous or anyway highly disordered, whereas the CdS bleb is crystalline in the case of dimers.

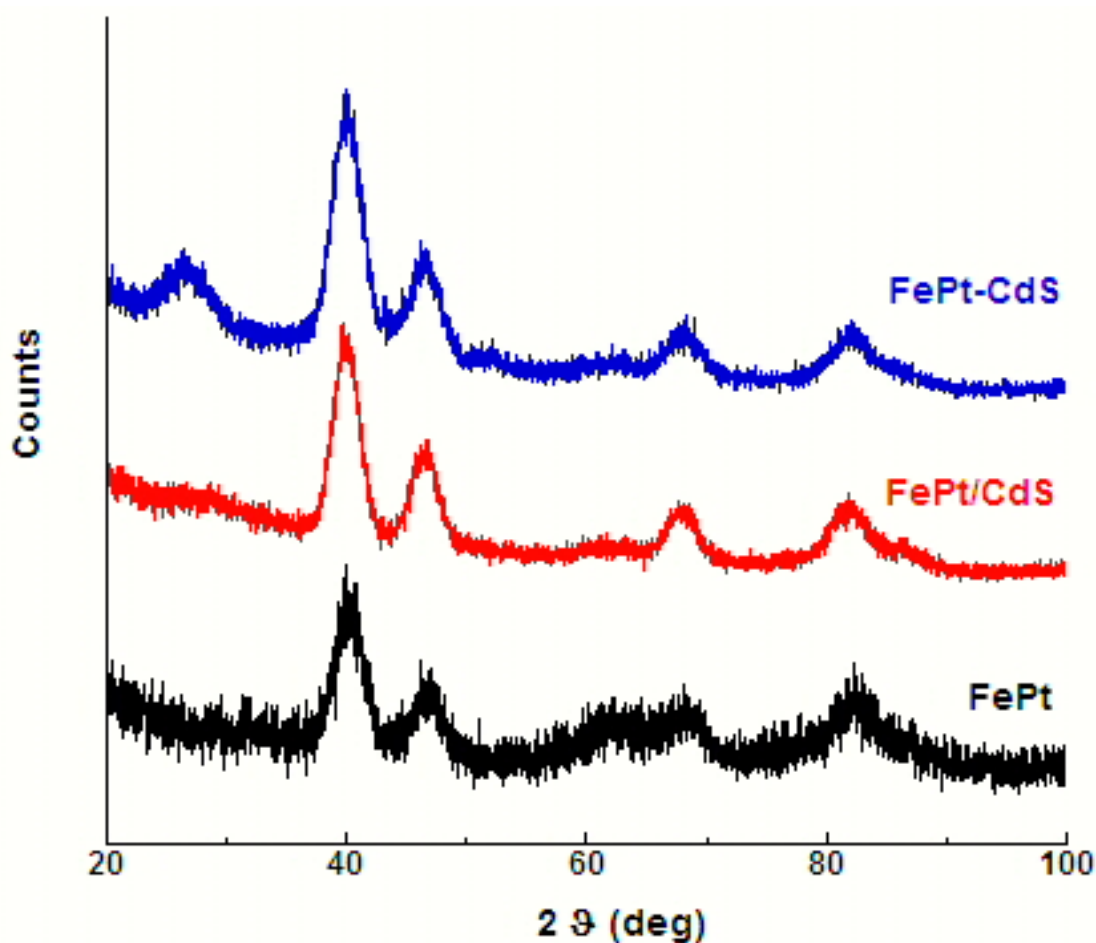


**Figure SI-5:** From bottom to top: XRD patterns ( $\text{Cu-K}\alpha$  radiation) of plain FePt nanoparticles, of FePt/CdS core/shell nanoparticles, and of the FePt-CdS dimers. For clarity the individual curves are shifted to higher count rates.

The same result was obtained for all those systems where we could isolate the different products at the different steps of the preparation, i.e. the core/shell samples do not show any diffraction peak in addition to the reflections due to the FePt alloy. As discussed in the manuscript, due to the very high reactivity for some systems only the final dimers could be isolated. The XRD patterns of all the dimer samples are reported in Figure SI-6 and show the presence of the reflections due to the FePt alloy as main contribution. In addition, in the angular range below  $\sim 38^\circ$  ( $2\theta$ ) where no peaks due to iron-platinum are found, extra features are observed, which are either broad or well-resolved reflections, depending on the semiconductor material present in the dimer.

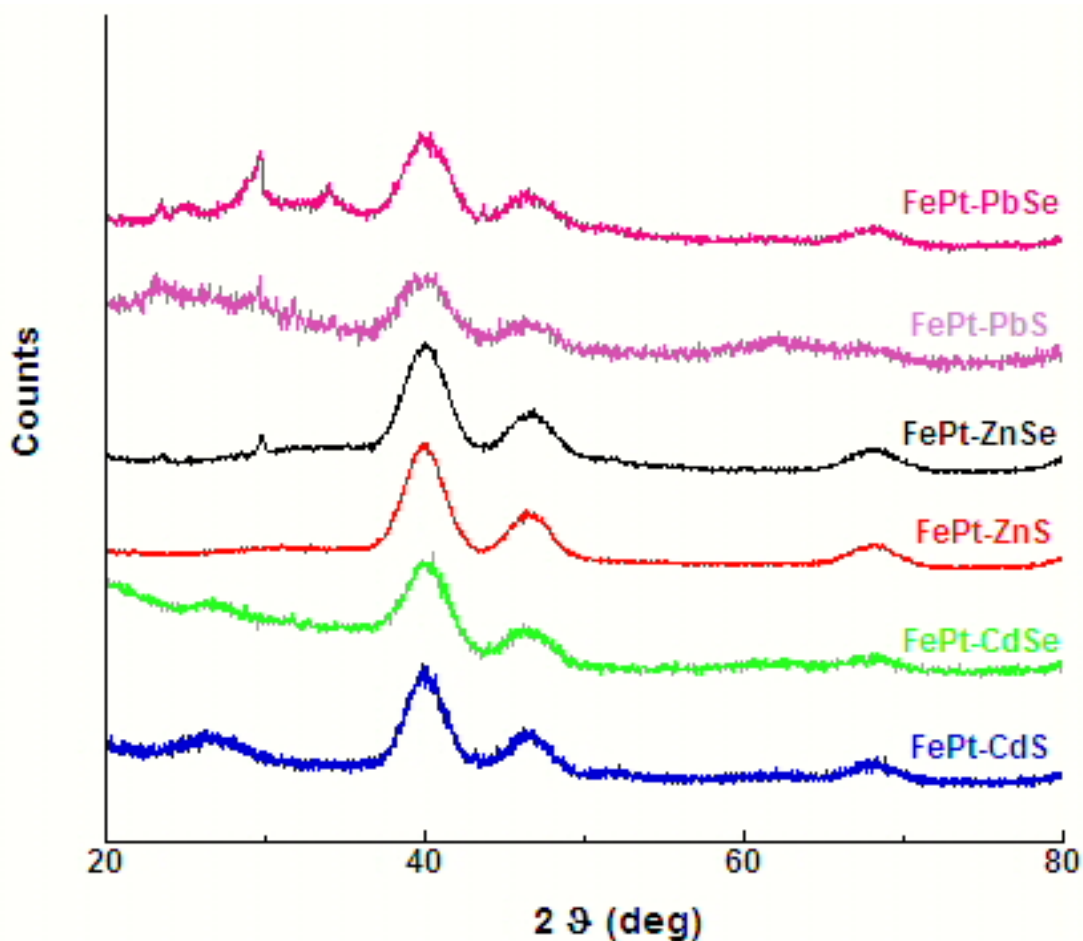


**Figure SI-6:** XRD patterns of all dimer samples ( $\text{Cu-K}_\alpha$  radiation). From bottom to top: FePt-CdS, FePt-CdSe, FePt-ZnS, FePt-ZnSe, FePt-PbS, FePt-PbSe. The individual curves are shifted towards higher count rates.

In the FePt-CdS and FePt-CdSe dimers a very broad peak can be associated to the formation of nanocrystalline CdS and CdSe respectively. The main reflections of the wurtzite and of the sphalerite structure lie at close angular values and therefore due to the peak broadening associated to the small nanocrystal size it is not straightforward to attribute unambiguously the crystal structure of the CdS and CdSe domain to the zinc blende or to the wurtzite structures. In the FePt-ZnS and FePt-ZnSe sample a halo is observed suggesting that the structure is more disordered or that the crystal domains are smaller, at the limit of detection of XRD technique ( $\sim 3$  nm). The FePt-PbS and FePt-PbSe dimers show sharper peaks which may be attributed to cubic PbS (PbSe) and to a lead-platinum alloy. This is particularly evident in the FePt-PbSe dimer, where the reflections which are not due to FePt can be attributed to the most intense peaks of PbSe and of an alloy richer in lead,  $\text{Pb}_4\text{Pt}$ . These data support the occurrence of diffusion of the atoms from the magnetic to the semiconductor domain (or vice versa) as suggested by magnetic measurements. Due to the extra line broadening of the XRD peaks related to small size effects no significant peak shift or broadening is observed in the reflections due to the FePt alloy due to potential compositional or disorder variations.

## II.2) HREM

To gain further insights on the crystal structure of the heterostructures, High Resolution Transmission Electron Microscopy (HRTEM) was performed at the TEMSCAN facility in Toulouse, France, on a JEOL JEM2100F microscope operating at a voltage of 200 kV and equipped

with a Field-Emission gun. Prior to observations, samples were deposited by drying a drop of the colloidal solution on top of a holey carbon-coated copper grid. In the HRTEM images of all the samples the FePt alloy core is clearly visible and the size and crystal lattice of the magnetic core is not significantly altered in the heterostructures with respect to the plain alloy nanocrystals. These data are in agreement with conventional TEM and XRD data. It is difficult to image the lattice fringes of both the semiconductor and the magnetic domain of a given dimer structure because it is unlikely to observe both domains under an appropriate zone axis. However, we have always observed crystalline semiconductor domains which have a less regular shape and broader size distribution compared to the magnetic domains. Figure SI-7 shows FePt-CdS and FePt-CdSe dimers where coexisting semiconductor and magnetic crystalline domains are visible. The d-spacings observed in the magnetic core are close to the value of 2.23 Å due to the 111 family of planes of the FePt alloy phase. In the semiconductor domains interplanar distances which are only found in the wurtzite structure are observed. In particular, in the FePt-CdS and in the FePt-CdSe dimers interplanar distances due to the 101 family of the wurtzite phase (expected at 3.16 Å and at 3.29 Å in the CdS and CdSe respectively) and which are not present in the sphalerite structure can be observed. The presence of the wurtzite phase is also supported by the observed zig-zag structures which are due to the presence of stacking faults often associated to the occurrence of the wurtzite phase. In all the investigated dimers there is no clear evidence of systematic epitaxial relationships between the magnetic and semiconductor domains, even if the low percentage of well oriented dimers does not allow to definitively conclude about such a matter. However, this result is somehow expected on the basis of the proposed mechanism of formation of the heterostructures, as crystallization of the semiconductor domain is concomitant to the dewetting process, and therefore is not due to the growth of the semiconductor on a given facet of the magnetic seed.

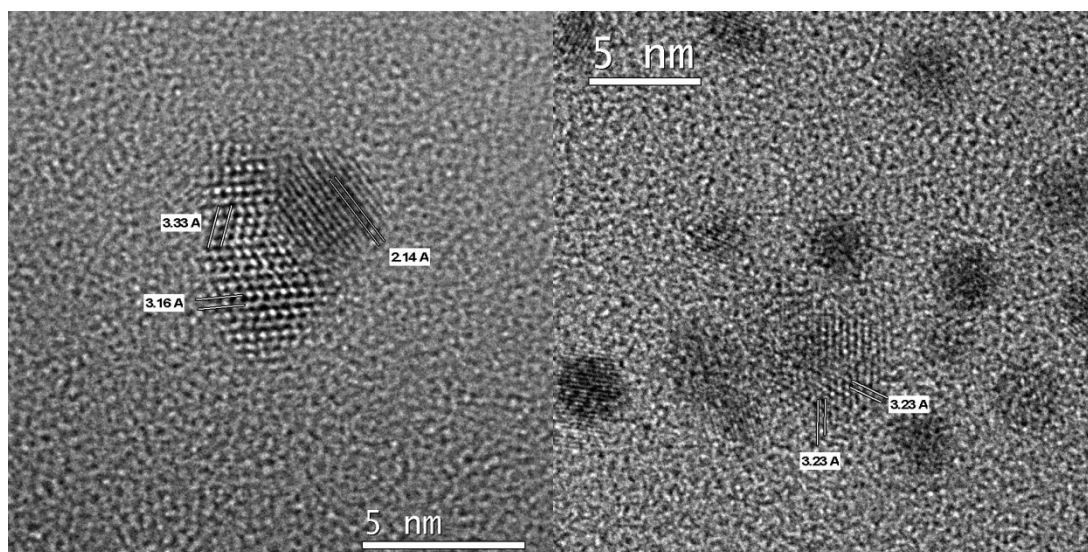


***Figure SI-7:*** HRTEM image of the FePt-CdS (left) and FePt-CdSe (right) dimers.

### III) Optical Characterization

For optical characterization an Agilent 8453 UV/vis absorption spectrometer and a Fluoromax-3 (Jobin Yvon Horiba) fluorescence spectrometer were used.

A comparison between the absorption spectra of free FePt nanoparticles and FePt-CdS dimers (both dissolved in chloroform) demonstrates that the dimers present a weak additional peak centered at ca. 400 nm, which is not present in the free iron platinum spectrum and can be explained as absorption feature of the CdS domain. From a calibration curve that relates the position of the absorption peak of free CdS nanoparticles to their size, we can estimate the diameter of the CdS domain as 3-4 nm [4]. Under UV light no emission was visible to the bare eye, but by using a fluorescence spectrometer several peaks could be detected (Figure SI-8). Fluorescence spectra were recorded after subsequent purification steps in order to demonstrate the possible contribution of surfactants to the fluorescence.

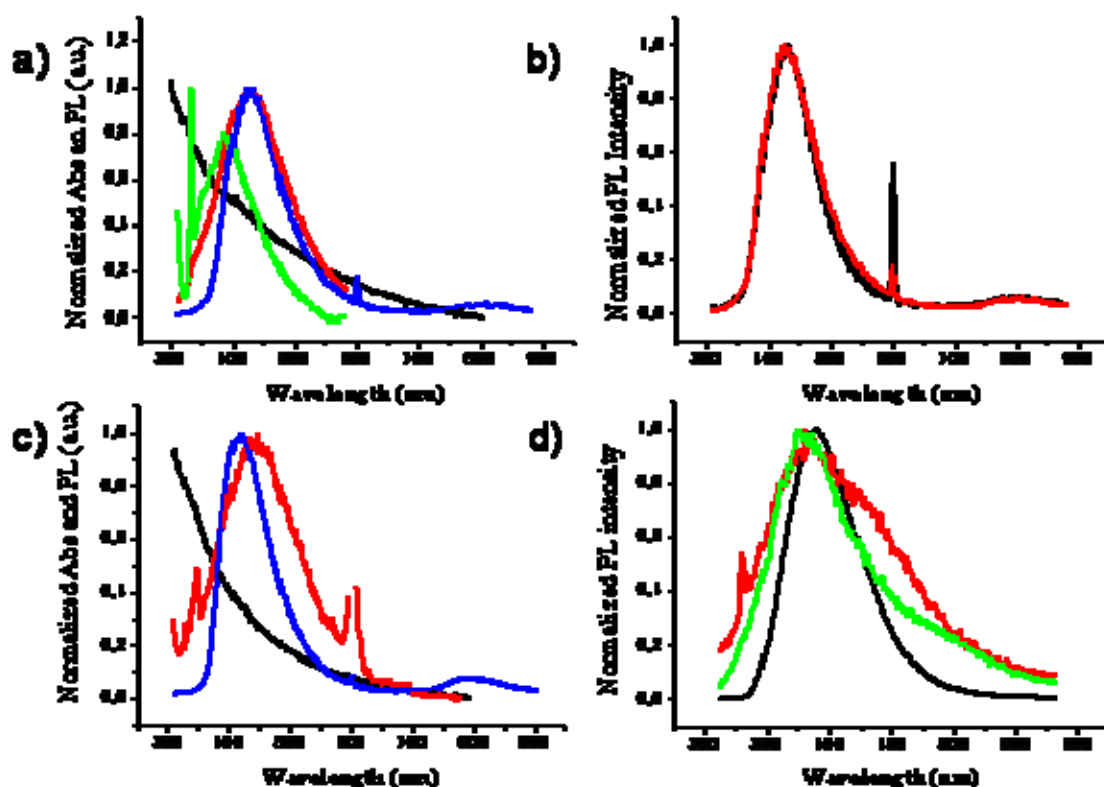


**Figure SI-8:** a) Normalized absorbance (Abs) and fluorescence (PL) spectra of FePt-CdS dimers: absorbance (black curve), fluorescence of the particles after one purification step involving precipitation and redissolution of the precipitate (red curve), fluorescence of the supernatant after the first precipitation which is not supposed to contain particles (blue curve). The peak at ca. 600 nm is a replica of the dominant peak at half the wavelength., fluorescence of the sample after several rounds of purification involving multiple precipitation and redissolution of the precipitate (green curve). b) Normalized fluorescence spectra of the supernatant of a solution of FeP/CdS core/shell particles (black curve) and FePt-CdS dimers (red curve). Both supernatants were collected after precipitation of the particle solution and should not contain particles (which are in the precipitate). c) Normalized absorbance and fluorescence spectra of FePt-CdSe dimers: absorbance (black curve), fluorescence of the particles after one purification step involving precipitation and redissolution of the precipitate (red curve), fluorescence of the supernatant after the first precipitation which is not supposed to contain particles and which is discarded (blue curve). d) Normalized fluorescence spectra of three different surfactants used for the nanoparticles synthesis: TOPO (red curve), oleylamine (green curve), and oleic acid (black curve). All of them were dissolved in chloroform before the measurement.

#### IV) Magnetic Characterization

The magnetic characterization (measurement of static Zero Field Cooled (ZFC) and Field Cooled (FC) magnetization, and of the isothermal hysteresis loop) of the ferromagnet-semiconductor dimeric systems was performed with a Quantum Design MPMS SQUID magnetometer equipped with a superconducting magnet producing fields up to 50 kOe. The samples were prepared by depositing the colloidal nanoparticles into a filter paper and afterward vacuum-drying. ZFC magnetizations were measured by cooling the samples in a zero magnetic field and then increasing the temperature in a static magnetic field of 50 Oe, while the FC curves were obtained by cooling the samples in the same magnetic field. For each system we obtained the blocking temperature ( $T_B$ ), defined as the temperature at which the main maximum of the ZFC curve appears, and the crossing temperature ( $T_{cross}$ ), in correspondence of which ZFC and FC curves are completely superimposed. Hysteresis loops were taken once the sample was cooled down at 2.5 K in a zero magnetic field. All the magnetization values are absolute, since they are referred to an unknown sample mass. From the hysteresis loops we could extrapolate the coercive field ( $H_c$ ), the ratio between the absolute magnetization ( $M_s$ ), extrapolated at high field, and the residual magnetization ( $M_r$ ) measured when the applied field ( $H$ ) is back to zero after the applied magnetic field had reached 5T.

#### V) References

1. Sun, S., et al., *Monodisperse FePt Nanoparticles and Ferromagnetic FePt Nanocrystal Superlattices*. Science, 2000. **287**(March 17): p. 1989-1992.
2. Gu, H., et al., *Facile One-Pot Synthesis of Bifunctional Heterodimers of Nanoparticles: A Conjugate of Quantum Dot and Magnetic Nanoparticles*. Journal of the American Chemical Society, 2004. **126**(18): p. 5664-5665.
3. PDF-2 File, JCPDS International Centre for Diffraction Data, 1601 Park Lane, Swarthmore, USA
4. Yu, W.W., et al., *Experimental Determination of the Extinction Coefficient of CdTe, CdSe, and CdS Nanocrystals*. Chemistry of Materials, 2003. **15**(14): p. 2854-2860.